Tribhuvan University Journal
Vol. 39, No. 2: 47-63, December 2024
Research Directorate, Tribhuvan University (TU),
Kathmandu, Nepal
DOI: https://doi.org/10.3126/tuj.v39i2.72878

CHARACTERIZATION OF COLD ATMOSPHERIC PRESSURE ARGON PLASMA IN DIELECTRIC BARRIER REACTOR

Akhilesh Kumar Singh[1,2], Rajesh Prakash Guragain[1], Asmita Shrestha[1], Ganesh Kuwar Chhetri[1], Santosh Dhungana[4], Hom Bahadur Baniya[3*], Deepak Prasad Subedi[1], Ujjwal Man Joshi[1]

[1]Department of Physics, School of Science, Kathmandu University, Dhulikhel, Nepal
[2]Tri-Chandra Multiple Campus, TU, Kathmandu
[3]Amrit Campus, TU, Kathmandu
[4]Central Department of Physics, TU, Kathmandu
**Corresponding author: hom.baniya@ac.tu.edu.np/hombaniya@gmail.com*

Received date: 8 Aug. 2024 – Accepted date: 28 Nov. 2024

ABSTRACT

The cold plasma has been produced, using high voltage and line frequency $(0-20\,kV, 50\,Hz)$ at atmospheric pressure. In this paper, the generation and characterization of plasma produced with argon gas in dielectric barrier discharge (DBD) reactor system is reported. The characterization of produced plasma has been done by electric and optical means using different techniques like current density method, power balance method, Boltzmann plot method, Stark broadening, line intensity ratio method and Saha-Boltzmann relation. Result reveled that electron density was of the order of $10^{11}\,cm^{-3}$, $10^{12}\,cm^{-3}$, $10^{11}\,cm^{-3}$, and $10^{16}\,cm^{-3}$ as determined by current density method, power balance method, Saha-Boltzmann relation and stark broadening approach respectively while excitation temperature of electron was estimated to be about 0.92 eV and 0.79 eV as determined by Boltzmann plot method and intensity ratio method respectively. The discharge power and energy consumed per cycle are determined using the Lissajous figure approach. The proper characterization of cold atmospheric pressure plasma (CAPP) is essential for seed treatment, polymer treatment, and water treatment.

Keywords: Stark Broadening approach, cold atmospheric pressure plasma, power balanced method, optical characterization, current density method, boltzmann plot

INTRODUCTION

Non-thermal cold atmospheric pressure plasmas or CAPPs, are used in industry, medicine, agriculture, and biology (Tanaka *et al.*, 2011; Ikehara *et al.*, 2013; Walsh *et al.*, 2008). CAPP is created in free space at atmospheric pressure, without the use of a vacuum apparatus. This is because it operates in a non-equilibrium state. In this state, the electrons in the plasma are highly energetic, but the overall gas temperature remains relatively low. This is achieved by applying an electric field that selectively energizes the electrons without transferring significant energy to the heavier ions and neutral particles. A CAPP generating process produces chemical effects rather than physical ones and does not cause thermal damage to the object. Since the CAPP system eliminates the need for a vacuum vessel, it make plasma processing easier. This opens up a wide range of plasma applications, where temperature, ion and electron densities, and plasma current control are critical to processing efficiency and safety. CAPP is produced using a noble gas or regular air, a single or double dielectric, and a metal electrode by using a high-voltage alternating current (AC) or direct current (DC) at ambient pressure (Lu *et al.*, 2014; Lu *et al.*, 2016). The properties of CAPP, which were produced with argon and helium, have been documented by various researchers (Lu *et al.*, 2021; Wu *et al.*, 2013). The operating parameters of plasma affect its electron density, temperature, and current; but the CAPP typically has an electron temperature of a few electron volts (Akatsuka *et al.*, 2009; Van Gessel *et al.*, 2012) and the electron density is in the range of $10^{11} - 10^{17}\ cm^{-3}$ (Yambe *et al.*, 2022; Kogelschatz, 2003).

Over the past 20 years, plasma that operates at atmospheric pressure has drawn more interest. Many research efforts focused on Dielectric Barrier Discharge (DBD) in the air at ambient pressure (Massines *et al.*, 2003; Sherman *et al.*, 2005). These days, these physical phenomena are widely recognized, and multiple studies have helped to understand and provide an explanation for the micro-discharge mechanism (Massines *et al.*, 2005; Lee *et al.*, 2005). Plasma technology is a highly adaptable and essential tool for material processing and product manufacturing across a variety of industries. Though often behind the scenes, it is both resource-efficient and transformative. Plasma processing is indispensable in fields like aerospace, automotive, biomedical, textiles, optics, polymers, and paper. The unique ability of non-thermal plasmas to interact with delicate materials and products has broadened its research and applications to areas

such as liquid treatment, organic tissues, and wound care, giving rise to plasma medicine.

In contrast to radiofrequency sources, which are far more costly, the cold plasma discharge generated at atmospheric pressure is also stable, even at low frequencies (Adamovich *et al.,* 2017). The majority of earlier research has employed radiofrequency power supplies, which are costlier than the power supply utilized in this investigation. The plasma produced in DBD reactor can be used to treat continuously for an extended period of time and DBD is designed using materials that are readily available locally. An economical method for producing cold atmospheric pressure argon plasma with several uses in seed treatment and biomedical research has been created (Baniya *et al.*, 2020; Wagner *et al.*, 2003). To innovate plasma sources and applications, as well as to control and enhance technologies, it is essential to understand fundamental processes and acquire quantitative knowledge of key plasma parameters, including electron density, species intensity, electron excitation temperature, Debye length, and others. In our work, a plasma device that can produce atmospheric plasma at low temperatures has been successfully constructed and some characters of discharge produced with argon gas at atmospheric pressure with 50 *Hz* line frequency were examined. This study is also focused on determination of plasma parameters like power consumption, electron density and electron excitation temperature by different approaches in a DBD reactor.

EXPERIMENTAL DETAILS

DBD Device Designation and Fabrication

The structure of the DBD reactor used in the experiment is as shown in Figure 1. It is made up of two solid copper cylinders that are 60 mm in diameter and 9 mm thick, serving as the electrodes. A dielectric barrier is a circular quartz plate with a radius of 45 mm and a thickness of 1 mm. Using the principle of screw gauze, the discharge width between the electrodes that provide the discharge volume can be adjusted. Electrodes, with the exception of the discharge area, are covered with Teflon to reduce localized heating and power loss resulting from edge effects and insufficient contact between the dielectric plates and electrodes. The lower and upper electrodes are attached to the upper and lower walls of a cuboidal wooden box that measures 300 mm by 100 mm by 120 mm and has polycarbonate glass sides on it. The distance between the electrodes can be adjusted by using nut bolts of a suitable size. Polycarbonate glass sides are used to

view the micro discharges that the reactor produces. Two holes of proper dimensions are made on polycarbonate glass for gas flow and to observe discharge. The two electrodes are kept at a horizontal plane using a spirit level.

Figure 1

Structure of dielectric barrier discharge reactor

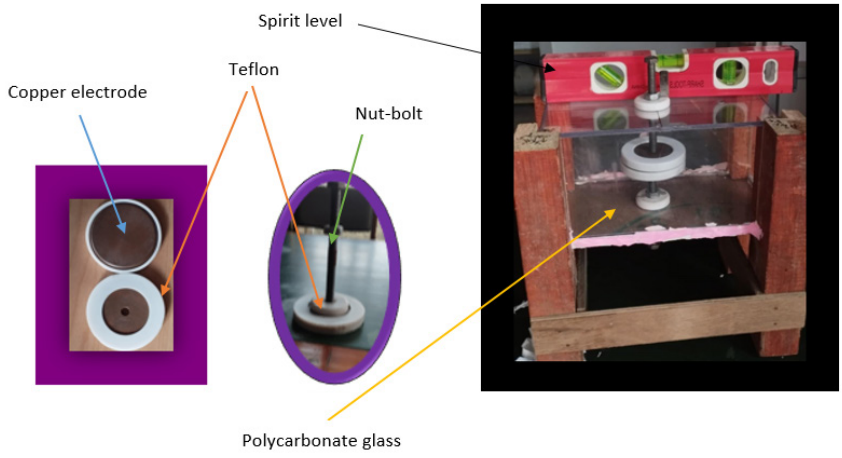

Experimental Setup

The schematic diagram of DBD parallel plane geometry used in the experiment is depicted in Figure 2. The two electrodes are subjected to 50 *Hz* AC power from the step-up transformer's output, and a 20 *M*Ω ballast resistor is connected in series with the top electrode, connected to high voltage, to limit the rate of flow of charge during the discharge. The discharge current was also estimated by feeding a voltage probe across a shunt resistor with a resistance of 10 *K*Ω. When measuring the voltage across electrodes, an upper electrode is linked to a 1000:1 high voltage probe (PINTEX HVP-28HF), and the lower electrode is earthed. To view the waveforms of the total discharge current and the applied voltage, a two-channel Tektronix TDS 2002, 60 *MHz* digital oscilloscope is employed. The electric characterization of discharge was done by using the Lissajous figure approach, current density method, and power balance method. The image of atmospheric pressure argon plasma produced in our own designed and fabricated DBD reactor system is shown in Figure 3. During the whole experiment, the rate of flow of argon gas in the DBD chamber is maintained

at 1 litre/minute. Figure 4 gives information about the discharge current and the voltage waveform at an input peak voltage of 6.6 *kV*. Optical characterization of the cold plasma was done by using the Boltzmann plot method, Line intensity ratio method, Saha-Boltzmann relation and Stark broadening approaches with the help of optical emission spectrometer (OES) (USB 2000+, Ocean Optics). The angle of acceptance and numerical aperture of the optical fiber used to collect light for the optical emission spectrometer (OES) are 28^0 and 0.465 respectively. The resolution of the spectrometer is 0.1*nm*.

Figure 2

Schematic diagram of parallel plate DBD (1. Optical emission spectrometer 2. Digital oscilloscope, 3. High voltage probe 4. Ballast resistor 5. Optical fiber 6. Upper electrode 7. Plasma discharge 8. Step up transformer 9. Shunt resistor 10. Lower electrode, 11. Dielectric barrier, 12. Ground, 13. Oscilloscope probe 14. Computer)

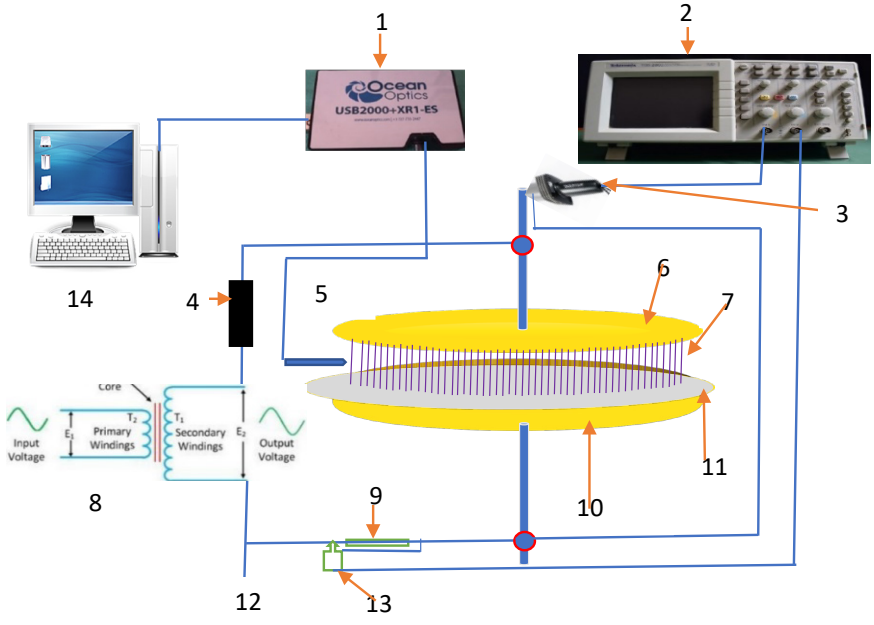

Data Analysis and Statistical Measure

The waveforms of the discharge current and voltage and optical spectra emitted by CAPP are noted at a discharge width of 2 *mm* at an alternating peak voltage of 6.6 *kV*. A convex lens is used to converge

spectra emitted by plasma so that a huge amount of radiation enters the optical fiber of OES. For optimal results, all data are collected thrice, with average values obtained for each distinct thickness and input sinusoidal voltage. The software Origin 2024b is used to analyze the data. The Bolsig+ software is used to find the mobility of electrons. Software called Minitab is employed in the statistical analysis.

Figure 3

Image of discharge

Figure 4

Photograph of voltage and current waveform

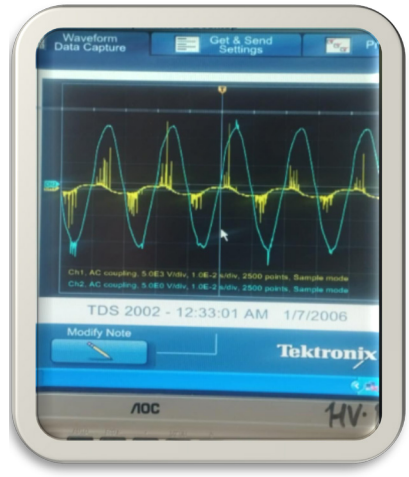

RESULTS AND DISCUSSION

Electrical Characterization of CAPP

Determination of energy and power consumption per cycle

The discharge current signal has some filaments superimposed on it, even though the applied voltage and discharge current are sinusoidal signals. Filaments in the current waveform are present in both cycles. There are no filaments at low discharge current amplitudes. Figure 5, which shows the applied voltage and discharge current at atmospheric pressure, demonstrates the connection between each current filament on the dielectric barrier material and a sequence of micro discharges (Kostov et al., 2009). One interpretation of Figure 5 would be that both circular electrodes released a number of micro discharges for each cycle of applied voltage. The power lost in the CAPP is calculated by using formula $P = f\int V(t)I(t)dt$ where, f is

line frequency. Figure 6 shows the parallelogram shaped Lissajous figure obtained at a peak voltage 6.6 *kV* for a discharge width of 2 mm. From the Lissajous figure approach and voltage and current waveform characteristics, it is found that the energy dissipated and power consumed in discharge per cycle is 1.67×10^{-4} J and 0.160 watt.

Figure 5

The voltage and current waveform

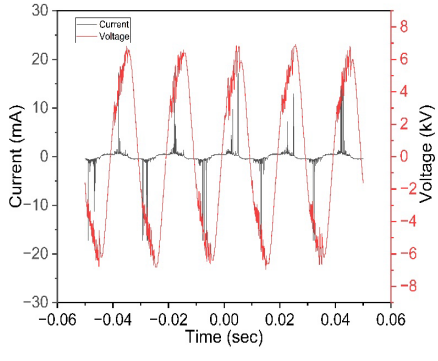

Figure 6

Q-V plot at peak volt 6.6 kV

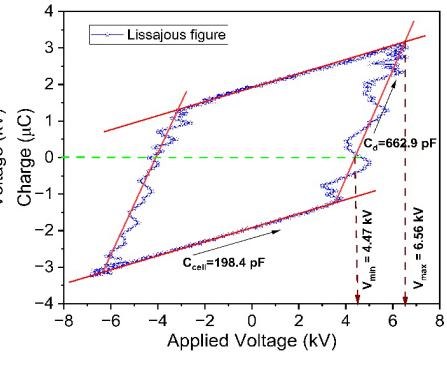

Determination of the density of electron by current density method:

The electron density n_e in discharge is found by using the equation: Current density $J^e_{con} = n_e \mu_e eE$. Here, E is the electric field intensity between in air gap which is obtained by dividing discharge voltage by discharge width. Hence, Electric field intensity in discharge region is found to be $E = \frac{V_D}{x} = \frac{3.13}{0.2} = 15.65 kVcm^{-1} = 1.565 \times 10^4 Vcm^{-1}$ .The reduced electric field in Townsend is found to be 58 *Td.* The electron mobility is found using Bolsig+ software by taking e-e collision and its value is found to be $250 cm^2 V^{-1} S^{-1}$. The average value of current is 15.8*mA* and the effective area of the discharge channel is found by multiplying an average number of filaments with area of a filament. The average radius of a single filament is taken as 100 μm (San Wong *et al.,* 2016). The number of the current peak is determined using origin soft-ware at a threshold height of 5% and the direct counting method. The average number of filaments at a peak voltage of 6.6 *kV* for a discharge width of 2 mm is found to be 229. Hence current density is found to be $0.115 Acm^{-2}$. Using the above equation, the density

of the electron is found to be $1.184 \times 10^{11}\, cm^{-3}$ which agrees with the report given by Yambe *et al.,* 2022.

Determination of the density of electron by power balance method:

The average power consumed by a capacitive coupled CAPP can be written as $\overline{P} = 2A_c n_e v_b E_{lost}$, where n_e being the density of electrons, E_{lost} being the loss of energy per cycle, A_c being the effective area of the discharge channel and v_b being the Bohm velocity. From the Lissajous figure shown in Figure 6, the average power consumed at a peak voltage of 6.6 *kV* for discharge width of 2 mm is 1.60 W. The Bohm velocity is $v_b = 2 \times 10^3 ms^{-1}$ and energy lost per cycle is $E_{lost} = 80 \times 10^{-19} J$ (Falahat *et al.,* 2018). The effective area of discharge channel is found to be $7.19 \times 10^{-2} cm^2$. Substituting all these values in the above mentioned equation, The electron density is found to be $6.95 \times 10^{12} cm^{-3}$ which agrees with the result given by Yambe *et al.,* 2022.

Optical Characterization of CAPP:

Determination of excitation temperature of electron by Boltzmann plot method

The spectra of the discharge captured from OES are depicted in Figure 7. These spectra have different species. For the Boltzmann plot method (Ciucci *et al.*, 1999; Griem *et al.*, 2005), we have used Ar I lines to estimate the excitation temperature of electrons in discharge. The observed four prominent argon lines 434.5 *nm*, 696.5 *nm*, 706.8 *nm,* and 772.3 *nm* are used to determine the excitation temperature of electron T_e. In a local thermodynamic equilibrium (LTE) approximation, the line intensity associated with the transition between two levels and of an atomic species can be written as follows:

$$I = \frac{Nhc}{U(T_e)} \frac{g_k A_{ki}}{\lambda} e^{\frac{-E_k}{K_b T_e}} \qquad [1]$$

Where λ = wavelength of transition, h = Planck's constant, c = speed of light in vacuum, E_k = energy of K^{th} level (Upper level), K_b = Boltzmann constant, A_{ki} = transitional probability, g_k = statistical weight factor of upper level, N = the total number density of the species and $U(T_e)$ = the partition function for the species emitted at the excitation temperature of electron T_e. With the help of logarithmic function, equation (1) reduces to

$$\ln\left[\frac{\lambda I}{hcg_k A_{ki}}\right] = -\frac{E_k}{K_b T_e} + \ln\left[\frac{N}{U(T_e)}\right] \quad [2]$$

This is the Boltzmann equation in the form of straight line with slope intercept form. Therefore, the excitation temperature of electron can be estimated from the slope of Boltzmann plot as shown in Figure 8. The values of intensities I of these spectral lines are obtained from spectra take form OES. The values of E_k, g_k, and A_{ki} for the selected lines are taken from the NIST atomic spectra database (Kramida *et al.,*2018) and are listed in Table 1. The slope of the linear fit of the experimental data gives the value $-1.086(eV)^{-1}$. Consequently, the excitation temperature of electron is 0.92 *eV* (Approx.10635 K) at peak voltage 6.6 *kV*.

Figure 7

Spectra of discharge at 50 Hz

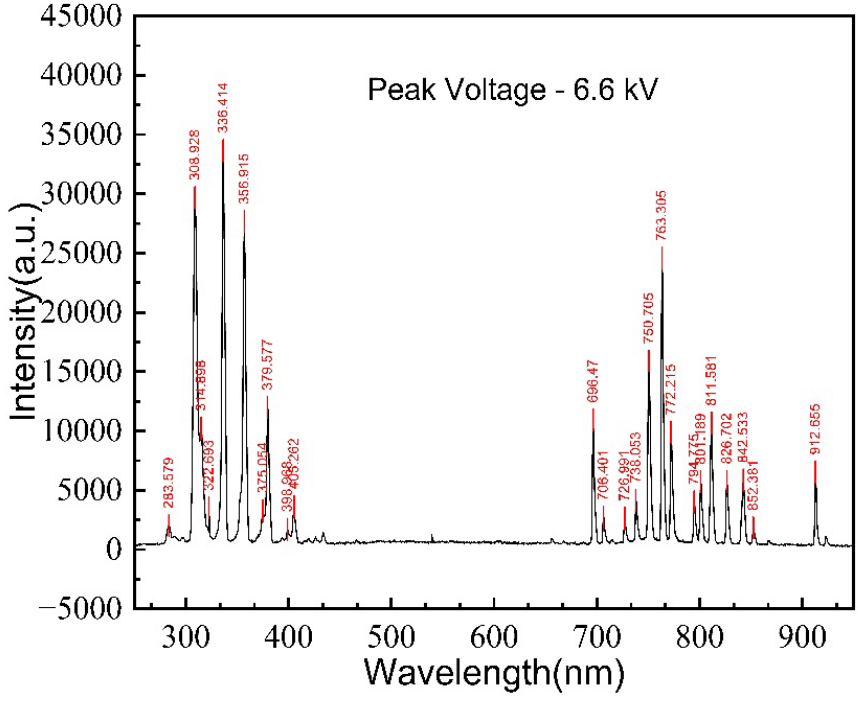

Figure 8

Boltzmann plot fit to estimate excitation temperature of electron at peak voltage $6.6\,kV$.

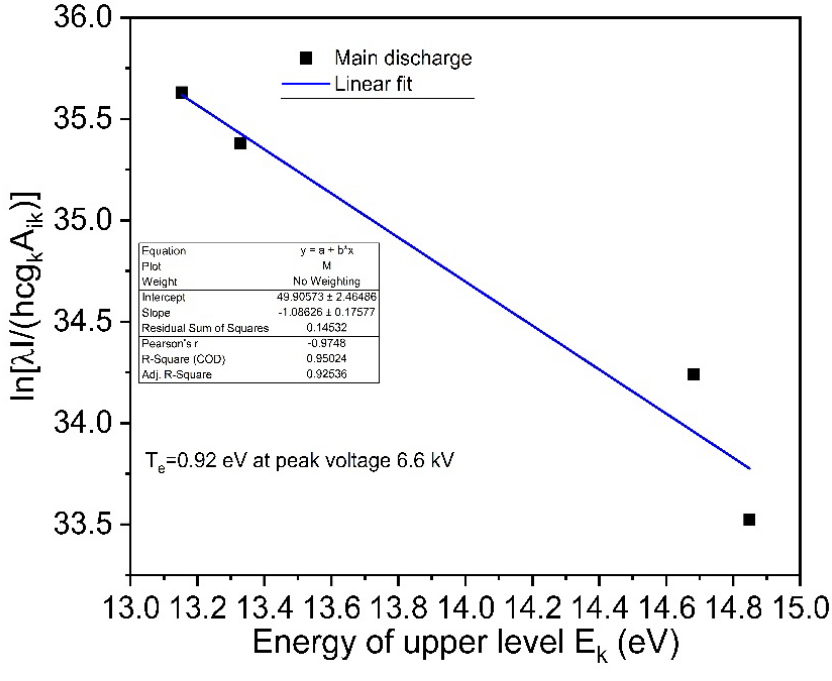

Table 1

The spectroscopic data of the observed Ar I lines for estimation of the excitation temperature of electron

Lines	Wavelength (nm)	Intensity (a.u)	Transitional probability (s^{-1})	Statistical weight	Energy (eV)
Ar I	434.5168	681.422	400000	5	13.327
Ar I	696.5431	12765.013	6400000	3	14.848
Ar I	706.8736	1536.444	2500000	6	13.153
Ar I	772.3761	11998.931	5200000	3	14.680

Determination of excitation temperature of electron by line intensity ratio method:

The spectral emission of CAPP in the region of 200-1100 *nm* is depicted in Figure 7. Argon lines exhibit distinct transitions, as seen by their presence in the wavelength range spanning from 696 *nm* to 850 *nm*. The transition of nitrogen is indicated by the peaks in the range of 330 –350 *nm*.

The sensitivity of this Boltzmann plot method depends on the ratio between K_bT_e and the values of energy at higher transition. The energy distribution at the top levels of Ar II was insufficient when compared with K_bT_e, and the findings were unrealistic when applied to the Ar II lines observed in the CAPP. Comparing the line intensities between various argon ionization degrees is required to achieve a higher level of accuracy. Therefore, we used the line intensity ratio approach to do an optical characterization of the discharge. Four lines were selected from the spectrum obtained from the CAPP as suitable for Ar I and Ar II. As mentioned in (Sarani *et al.*, 2010; Yambe *et al.*, 2016), the following working formula is utilized to get the electron temperature:

$$\frac{R_1}{R_2}=\frac{I_1/I_2}{I_3/I_4}=\left(\frac{A_{mn}}{A_{pq}}\right)\left(\frac{g_m}{g_p}\right)\left(\frac{\lambda_{pq}}{\lambda_{mn}}\right)\left(\frac{A_{uv}}{A_{wx}}\right)\left(\frac{g_u}{g_w}\right)\left(\frac{\lambda_{wx}}{\lambda_{uv}}\right)\exp\left[-\frac{E_m-E_p-E_w+E_u}{K_bT_e}\right] \quad [3]$$

In equation (3), R = the ratio of the intensities of two lines, I = the intensities of spectral lines, A_{ji}= the transitional probability of the transition $i\rightarrow j$, g_i = the statistical weight of the upper level, λ = the wavelength of line radiation, E_i= the energy of upper level, K_b = the Boltzmann costant and T_e = excitation temperature of an electron. We obtained the values of λ and I from observations and the values of A_{ji}, g_i and E_i from the NIST atomic spectra database (Kramida *et al.,*2018).

Table 2

Wavelength and intensity of Ar I and Ar II line at $6.6\,kV$.

Lines	Wavelength (nm)	Intensity (a.u)	Transitional probability (s^{-1})	Statistical weight	Energy (eV)
Ar I	696.543	11850.674	6.4×10^6	3	13.327
Ar I	794.817	5172.608	1.86×10^7	3	13.282
Ar II	322.597	4564.233	2.1×10^6	4	23.103
Ar II	375.048	4012.450	1.0×10^5	4	19.762

Table 2 gives the specific wavelength and the proper values of different parameters from the NIST atomic database (Kramida *et al.,* 2018). On substituting these values equation (3) can be expressed as

$$\frac{R_1}{R_2}=2.41\times10^{-2}\exp\left[\frac{3.30}{K_bT_e}\right] \quad [4]$$

When the graph is plotted between $\frac{R_1}{R_2}$ of equation (4) against different temperatures of electron in the range 0 to 2 eV, figure 9 is obtained.

The ratio of intensities of these specific wavelengths $\frac{I_1/I_2}{I_3/I_4}$ was 2.01 at 6.6 *kV.* Hence from the Figure 9, the excitation temperature of electron is found to be about 0.79 eV (approx..9133K).

Figure 9

Graph of intensities ratio of corresponding wavelength Vs K_bT_e

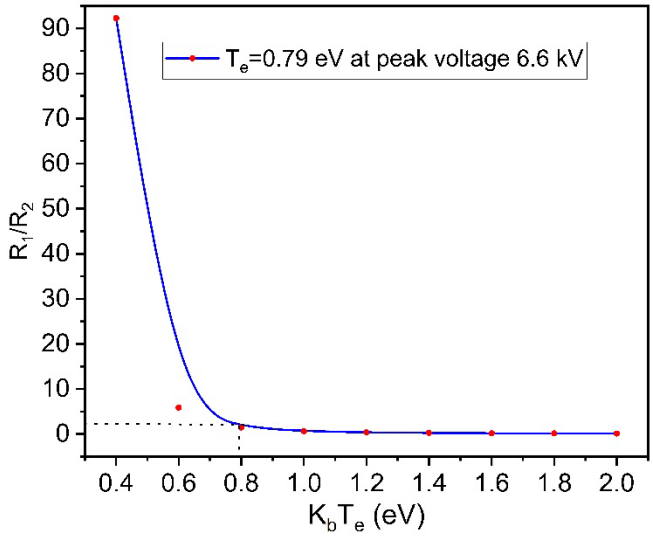

Determination of density of electron by the Saha-Boltzmann relation

This part now computes the electron density n_e using the average electron excitation temperature $T_e = 0.79\,eV$ obtained from line intensity method in filamentary modes. By necessity, partial local thermal equilibrium (PLTE) must exist in order to use the Saha equation (Balcon *et al.,* 2007). For the filamentary mode, one can assume PLTE between the top levels of each transition, assuming that the main processes in the discharge are radiative recombination and collisional ionizations. In the direction of observation, it is also crucial to consider that the source is optically thin. The Saha equation can be expressed as:

$$n_e = 2\left(\frac{I_+}{I_-}\right)\left(\frac{\lambda_+}{\lambda_-}\right)\left(\frac{A_-}{A_+}\right)\left(\frac{g_-}{g_+}\right)\left(\frac{2\pi m_e K_b T_e}{h^2}\right)^{\frac{3}{2}} \exp-\left[\frac{E_+ - E_- + E_i}{K_b T_e}\right] \quad [5]$$

Where I_+ = intensity of Ar II (375.048 nm) lines transition (4p-3d) and I_- = intensity of Ar I (794.817 nm) lines transition $4p - 4s$. λ, A and g are the wavelength, transitional probabilities (Einstein coefficient) and statistical weight (upper level) of the corresponding transition respectively. All the values of quantities present in right hand side of above equation are present in Table 1. The ionization potential of argon E_i is $15.760eV$. From these values, equation (5) gives the density of electron as 1.28×10^{11} cm^{-3} which agrees with the result given by Wu *et al.,* 2016.

Determination of Density of Electron by Stark Broadening Approach

According to Gigosos *et al*. (1996), the Stark broadening of the Ar spectral line determines the electron density of CAPP in the filamentary mode. Along with Stark broadening, other factors that contribute to the broadening of the Ar spectral line profile include Doppler broadening, van der Waals broadening, and instrumental broadening. It is usually easy to disregard both the resonance and natural broadening in high-density plasmas. Consequently, the Ar spectral line profile is often broadened as a result of these components' combined influence. Though the variation in electron temperature can be disregarded for atmospheric pressure plasma in argon, the Stark broadening is theoretically dependent on both electron temperature and density (Dong *et al.*, 2005). As a result, only the filamentary mode was utilized as a density diagnostic using the Stark broadening method. Here, each broadening mechanism operates independently of the others. The combined line profile is the convolution product of the line patterns of each mechanism. The Lorentzian nature of the Stark broadening is established. The Lorentzian fit of the argon line 696.5 *nm* at a peak voltage of 6.6 *kV* is shown in Figure 10. The value of the full width of half maximum (FWHM) of spectral line 696.5 *nm* at a peak voltage of 6.6 *kV* is 2.06 $\AA$. The electron density for the filamentary mode is determined using the equation $\Delta\lambda = 2\times10^{-11} n_e^{\frac{2}{3}}$, and the electron density is found to be $3.3\times10^{16} cm^{-3}$. This value is consistent with the outcome of Stark broadening on an argon line (Dong *et al*., 2005).

Figure 10

Lorenzian fit of Ar 696.5 nm line in filamentary mode

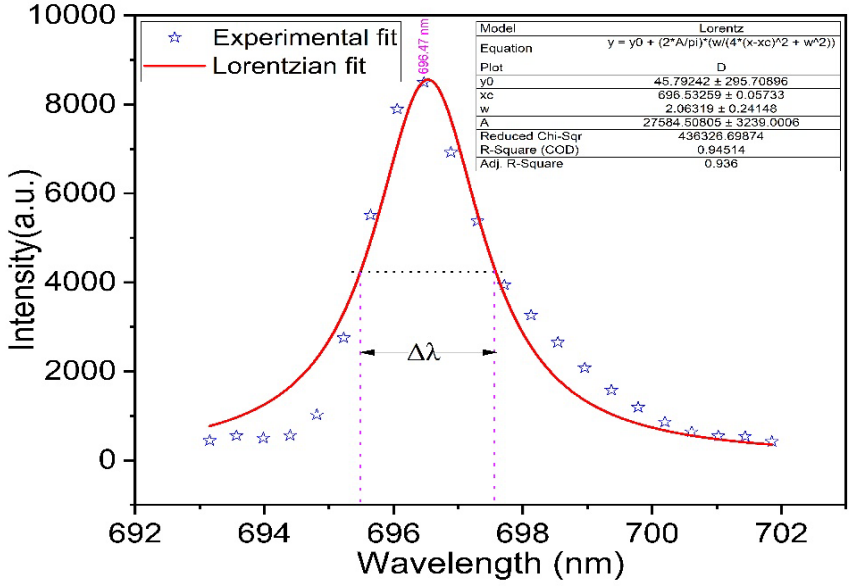

CONCLUSION

The experimental findings reported in this study demonstrate that non-thermal plasma can be produced by dielectric barrier reactor at atmospheric pressure with a line frequency of 50 Hz. Because of the small gap size and the rapid fluctuation of plasma properties, identifying the plasma at atmospheric pressure is frequently difficult. We have demonstrated, however, that optical emission spectroscopy may provide a reliable estimate of both the electron temperature and density. The electron density obtained by the current density method, Saha - Botzman relation, and Power balance method agrees well with the order of $10^{11} cm^{-3}$ while electron density obtained from Stark broadening is of the order of $10^{16} cm^{-3}$. The excitation temperature of electron as determined by the Boltzmann plot and line intensity ratio method are $0.92eV$ and $0.79eV$ at a peak voltage of 6.6 kV which satisfies the temperature of cold plasma. The characteristics of this discharge at atmospheric pressure were similar to those of the traditional capacitive radiofrequency discharge at lower pressure. Without the need for a chamber, the discharge operates at atmospheric pressure, making it

suitable for quick on-line surface treatment of polymers, seed treatment, and water treatment without causing vacuum compatibility issues.

ACKNOWLEDGEMENTS

The corresponding author was supported by the University Grant Commission (UGC), Nepal, for providing a small RDI Grant through Grant No: SRDIG-078/079-S&T-17. The authors would like to acknowledge all the researchers of the Department of Physics, School of Science, Kathmandu University for their invaluable help and support.

REFERENCES

Adamovich, I., Baalrud, S. D., Bogaerts, A., Bruggeman, P. J., Cappelli, M., Colombo, V., ... & Vardelle, A. (2017). The 2017 Plasma roadmap: Low temperature plasma science and technology. *Journal of Physics D: Applied Physics*, *50*(32), 323001.

Akatsuka, H. (2009). Excited level populations and excitation kinetics of nonequilibrium ionizing argon discharge plasma of atmospheric pressure. *Physics of Plasmas*, *16*(4).

Balcon, N., Aanesland, A., & Boswell, R. (2007). Pulsed RF discharges, glow and filamentary mode at atmospheric pressure in argon. *Plasma Sources Science and Technology*, *16*(2), 217.

Baniya, H. B., Guragain, R. P., Baniya, B., & Subedi, D. P. (2020). Experimental study of cold atmospheric pressure plasma jet and its application in the surface modification of polypropylene. *Reviews of Adhesion and Adhesives*, *8*(2), S1-S14.

Ciucci, A., Corsi, M., Palleschi, V., Rastelli, S., Salvetti, A., & Tognoni, E. (1999). New procedure for quantitative elemental analysis by laser-induced plasma spectroscopy. *Applied spectroscopy*, *53*(8), 960-964.

Dong, L., Ran, J., & Mao, Z. (2005). Direct measurement of electron density in microdischarge at atmospheric pressure by Stark broadening. *Applied Physics Letters*, *86*(16).

Gigosos, M. A., & Cardeñoso, V. (1996). New plasma diagnosis tables of hydrogen Stark broadening including ion dynamics. *Journal of Physics B: Atomic, Molecular and Optical Physics*, *29*(20), 4795.

Griem, H. R. (2005). *Principles of plasma spectroscopy,* (p. 386).

Ikehara, Y., Sakakita, H.,Shimizu, N., Ikehara, S.& Nakanishi, H.(2013). Formation of membrane-like structures in clotted blood by mild plasma treatment during hemostasis. *Journal of Photopolymer Science and Technology*, *26*(4), 555-557.

Kogelschatz, U. (2003). Dielectric-barrier discharges: their history, discharge physics, and industrial applications. *Plasma chemistry and plasma processing*, *23*(1), 1-46.

Kostov, K. G., Honda, R. Y., Alves, L. M. S., & Kayama, M. E. (2009). Characteristics of dielectric barrier discharge reactor for material treatment. *Brazilian Journal of Physics*, *39*, 322-325.

Kramida, A., Ralchenko, Y., & Reader, J. (2018). NIST atomic spectra database. *NIST standard reference database*, *78*.

Lee, D., Park, J. M., Hong, S. H., & Kim, Y. (2005). Numerical simulation on mode transition of atmospheric dielectric barrier discharge in helium-oxygen mixture. *IEEE transactions on plasma science*, *33*(2), 949-957.

Lu, X., Naidis, G. V., Laroussi, M. A., & Ostrikov, K. (2014). Guided ionization waves: Theory and experiments. *Physics Reports*, *540*(3), 123-166.

Lu, X., Naidis, G. V., Laroussi, M., Reuter, S., Graves, D. B., & Ostrikov, K. (2016). Reactive Species in non-equilibrium atmospheric-pressure plasmas: Generation, transport, and biological effects. *Physics Reports*, *630*, 1-84.

Lu, X., Liu, D., Xian, Y., Nie, L., Cao, Y., & He, G. (2021). Cold atmospheric-pressure air plasma jet: Physics and opportunities. *Physics of Plasmas*, *28*(10).

Massines, F., Segur, P., Gherardi, N., Khamphan, C., & Ricard, A. (2003). Physics and chemistry in a glow dielectric barrier discharge at atmospheric pressure: diagnostics and modelling. *Surface and Coatings Technology*, *174*, 8-14.

Massines, F., Gherardi, N., Naudé, N., & Ségur, P. (2005). Glow and Townsend dielectric barrier discharge in various atmosphere. *Plasma physics and controlled fusion*, *47*(12B), B577.

San Wong, C., & Mongkolnavin, R. (2016). *Elements of plasma technology*. Springer Singapore. Falahat, A., Ganjovi, A., Taraz, M., Ravari, M. R., & Shahedi, A. (2018). Optical characteristics of a RF DBD plasma jet in various Ar/O 2 mixtures. *Pramana*, *90*(2), 27.

Sarani, A., Nikiforov, A. Y., & Leys, C. (2010). Atmospheric pressure plasma jet in Ar and Ar/H2O mixtures: Optical emission spectroscopy and temperature measurements. *Physics of Plasmas*, *17*(6).

Sherman, D. M. (2005). The transition from a filamentary dielectric barrier discharge to a diffuse barrier discharge in air at atmospheric pressure. *Journal of Physics D: Applied Physics*, *38*(4), 547.

Tanaka, H., Mizuno, M., Ishikawa, K., Nakamura, K., Kajiyama, H., Kano, H., ...Hori,M.(2011). Plasma-activated medium selectively kills glioblastoma brain tumor cells by down-regulating a survival signaling molecule, AKT kinase. *Plasma Medicine*, *1*(3-4).

Van Gessel, A. F. H., Carbone, E. A. D., Bruggeman, P. J., & Van Der Mullen, J. J. A. M. (2012). Laser scattering on an atmospheric pressure plasma jet: disentangling Rayleigh, Raman and Thomson scattering. *Plasma Sources Science and Technology*, *21*(1), 015003.

Wagner, H. E., Brandenburg, R., Kozlov, K. V., Sonnenfeld, A., Michel, P., & Behnke, J. F. (2003). The barrier discharge: basic properties and applications to surface treatment. *Vacuum*, *71*(3), 417-436.

Walsh, J. L., & Kong, M. G. (2008). Frequency effects of plasma bullets in atmospheric glow discharge. *IEEE Transactions on Plasma Science*, *36*(4), 954-955.

Wu, S., Gou, J., Lu, X., & Tang, M. (2016). A 3.4-$\mu\text {m} $-Sized Atmospheric-Pressure Nonequilibrium Microplasma Array With High Aspect Ratio and High Electron Density. *IEEE Transactions on Plasma Science*, *44*(11), 2632-2637.

Wu, S., Xu, H., Lu, X., & Pan, Y. (2013). Effect of Pulse Rising Time of Pulse dc Voltage on Atmospheric Pressure Non-Equilibrium Plasma. *Plasma Processes and Polymers*, *10*(2), 136-140.

Yambe, K., & Satou, S. (2016). Investigation of helium plasma temperature in atmospheric-pressure plasma plume using line pair method. *Physics of Plasmas*, *23*(2).

Yambe, K., Izumida, T., & Akatsuka, H. (2022). Estimation of electron density and temperature by continuum spectrum in a moving atmospheric-pressure nonthermal-equilibrium argon plasma bullet. *IEEE Transactions on Plasma Science*, *50*(10), 3593-3601.